Space charge formation in the system with hopping ionic conductivity as the electric power generation at low temperature gradients

Michael Reznikov
Senior Member, IEEE
Physical Optics Corporation
1845 205th Street
Torrance, CA 90501, USA
mreznikov@poc.com

Paul Wilkinson
Physical Optics Corporation
1845 205th Street
Torrance, CA 90501, USA
pwilkinson@poc.com

***Abstract* -- The hopping charge transfer in the ion-conductive material is analyzed and experimentally investigated as the thermoelectric power generation. The physical model for the phenomenon as well as experimental results are analyzed in means of practical implementation with power conversion for energy harvesting from heat wastes or wide-spectrum solar radiation. Provided analysis addresses the thermoelectric efficiency, the power conversion efficiency and conditions for the optimal application as a low temperature thermoelectric converter.**

***Index Terms*—Electrochemical processes, Polymer gels, Thermoelectricity**

I. INTRODUCTION

There is the need in advanced thermoelectric (TE) technologies to recover waste heat from buildings, industry, and vehicles because typical low-temperature waste heat flows do not provide enough difference in temperature to support conventional thermoelectric power generators. For example, today only in USA, 29 quadrillion kJ of thermal energy is vented annually by power plants, buildings, and industrial complexes into the atmosphere, lakes, and rivers. This staggering amount of thermal loss comes from the conversion of fuel to electric power, and it exceeds the amount of energy consumed annually both by the U.S. transportation sector and by the entire Japanese economy [1]. About a quarter of this waste energy is produced by buildings and industrial processes [2]. This energy, in the form of medium- to low-temperature gases or low-temperature liquids (<120°C), is mostly wasted [1-3] because this low temperature does not provide a steep enough difference in temperature to support conventional thermoelectric power generators [4-6].

The presented work describes a new thermoelectric technology based on the thermally driven diffusion of protons in a nanoporous structure. A similar phenomenon provides superior sensitivity to thermal fluctuation in the receptors of marine sharks and skates (rays), which contain extracellular hydrogel [7]. These ionic structures can be mimicked by natural and synthetic gels, which exhibit significant TE voltage in the temperature gradient, a few mV/K at low and room temperatures [8]. Synthetic nanoporous materials, for example – Nafion® from DuPont Corp., currently are commercially available to address the demands of fuel cell technology, where they are used as proton-conductive membranes. According to our model [9], in these materials protons are thermally transferred between hopping places separated by an energy barrier and the temperature gradient creates an asymmetric transfer of charge carriers, which in turn generates the electric potential difference between the electrodes.

II. THEORY

The model of thermoelectricity in nanoporous ionic conductors without accounting for effects at electrodes [9] assumes an open circuit, a low electric field, and a small distance between electrodes. This model accounts for the low thermal effect on the concentration of mobile ions, but a significant effect of temperature on the mobility of ions due to the thermodiffusion mechanism of charge transfer [10]. Model is based on the Grotthuss diffusion mechanism in proton mobility, the dynamic capturing and release of protons that constitute the basic mechanism of proton transfer in nature. This mechanism comprises the cyclic isomerization between two forms of protonated water, H_3O^+ and $H_5O_2^+$, which is coupled to hydrogen-bond dynamics in the second solvation shell of the H_3O^+. As a result, the Grotthuss mechanism is the proton-hopping mechanism where each oxygen atom simultaneously passes and receives a single hydrogen atom. Because of the interaction with the wall of a pore, localized water molecules create deeper traps for protons than those in the bulk water [11]. As a result, proton conductivity is higher in the bulk water, while the hopping between the molecules attached to the wall is more sensitive to the temperature, due to the higher activation barrier, W_b. If there is no temperature gradient, the average net exchange flow (per unit of volume) is zero, and the transfer rate in any direction (for isotropic material, of course) may be presented as

$$j_{ij} = Const \cdot n \cdot f(T) \cdot \exp\left(-\frac{Wb}{kT}\right), \quad (1)$$

where $f(T)$ is the frequency of oscillations of the ion

The work was supported by DOE grant DE-SC0006283.

(attempts to go over the barrier W_b). Because the exponential component in Eq. (1) depends on the local barrier height and temperature, the hopping transfer is affected by the gradient of the electric potential, φ, or/and the temperature T. For example, the electric field, $E=- d\varphi/dx$, leads to the asymmetry of the energy barrier, which, in turn, results in the net exchange flow

$$j = j_{12} - j_{21} = Const \cdot f \cdot n \cdot \exp\left(-\frac{W_b}{kT}\right) \cdot \sinh\left(-\frac{q \cdot \delta}{2kT}\frac{d\varphi}{dx}\right). \quad (2)$$

The effect of electric field should be accounted for the steady state when the space charge and corresponding thermoelectric voltage are developed.

The temperature gradient leads to the thermoelectric generation of a space charge formed by charge carriers. Assuming an open circuit and uniform temperature gradient ($dT/dx = \alpha$), the distribution of charge carriers may be presented as

$$n = n_0 \exp\left[\frac{2W_d + q\delta E}{2k}\left(\frac{1}{T_0 + \alpha x} - \frac{1}{T_0}\right)\right], \quad (3)$$

where n_0 and T_0 are the proton density and temperature at the cold end, respectively, and $W_d = W_{dis}+W_b$ includes the enthalpy of dissociation, W_{dis}, to account for proton generation at varied temperatures. Now the gradient of the electric field can be expressed by the charge density in the Poisson equation $\frac{dE}{dx} = \frac{q}{\varepsilon\varepsilon_0}\frac{n - n_0}{2}$, and the thermoelectric voltage at the small distance, d, is

$$U(d) = \frac{qW_d n_0}{12\varepsilon\varepsilon_0 kT}\frac{\Delta T}{T}d^2, \quad (4)$$

where the difference in temperature $\Delta T = \alpha d$ and T is the average temperature over the distance d, which is small enough to satisfy the suppositions of weak electric field created by the thermoelectric voltage. Therefore, Eq. (4) can be considered as a linear approximation of the thermoelectric voltage per the unit of length in the temperature gradient.

Eq. (3) was numerically evaluated without the necessity of analytic simplifications. This derived function E(x) and therefore the integral of it, U(x). Fig. 1 presents the result of such a numerical simulation for an initial concentration of protons, $n_0 = 10^7$ cm^{-3}) at a varied temperature gradient, hopping activation energy 0.08 eV (≈3 kT at the temperature 300 K), and an average spacing between hopping places of 1 nm. The concentration of protons, n_0, was chosen for the matching of simulation results to experimental data. This concentration is 6000 times lower than that in the neutral water (10^{-7} mol/liter or $6\cdot10^{10}$ cm^{-3}) that supports the suggestion that only water molecules attached to pore wall provide the hopping of protons for the thermoelectric effect.

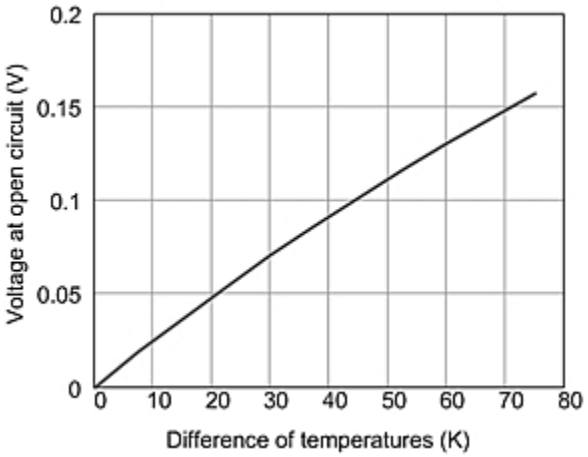

Fig. 1. Numerically simulated voltage at open circuit if the distance between electrodes is 2.5 cm

The results of this numerical simulation show that the voltage at open circuit almost linearly depends on the temperature difference at electrodes, while typical experimental results show significant non-linearity. Therefore the model should be extended to account for additional processes such as the thermogalvanic effect from the thermally activated electrochemical exchange on electrodes and the contact barrier for oxidation of hydrogen on the cathode. Fig. 2 shows a schematic of processes comparable to those in the loaded device.

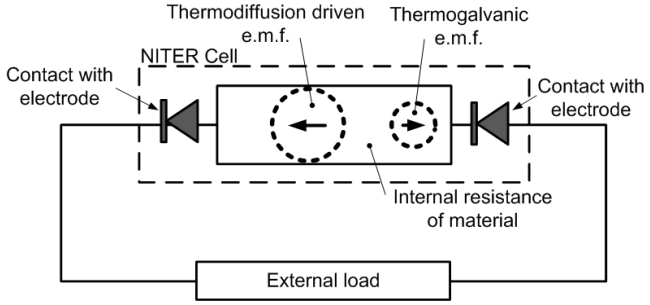

Fig. 2. Schematic showing processes comparable to those in a nanoporous protonic thermoelectric cell.

Thermogalvanic e.m.f. [12-13] works against the thermodiffusion driven e.m.f., which in fact creates the described thermoelectric effect. The contact of ionic conductor with electrodes is mostly responsible for the non-linearity of thermoelectric voltage in loaded circuit. Both these e.m.f.'s depend on the material of electrodes and should be evaluated for each couple of ionic conductor and electrode materials.

Typically, [14] the thermogalvanic e.m.f. is defined simply as $E_{oc} = (d\phi_0/dT)\Delta T$, where ϕ_0 is the potential of one half-cell due to the potential difference at the electrode-electrolyte interface:

$$\phi_0 = \phi_{00} + \frac{RT}{zF}\ln a_i \ , \qquad (5)$$

where ϕ_{00} is a standard electrode potential, R is a molar gas constant, T is an absolute temperature, z is the number of charges of the ion, F is the Faraday's constant, and a_i is the activity of the ion. In the case of protons (hydronium ions), which are the product of thermal dissociation of the solvent (water), the activity of ions is temperature-dependent, so the coefficient $d\phi_0/dT$ also depends on temperature.

The model, described by Eqs. (1-4) for the open circuit condition, may be expanded to the loaded regime. In this case, the condition for density of electric current, j, in the open circuit (j = 0) is replaced by the condition of continuity for electric current (dj/dx = 0), which converts the balance of the drift and diffusion currents to the differential equation

$$\frac{\partial n(T)}{\partial x}E + n(x,T)\frac{dE}{dx} + \frac{kT}{q}\frac{\partial^2 n(T)}{\partial x^2} = \gamma n\frac{dT}{dx} + \gamma\frac{\partial n(T)}{\partial x}T \ , \quad (6)$$

where γ is the coefficient of thermodiffusion ($j_{td} = \gamma n \cdot dT/dx$) and the concentration of protons, n, depends on the distance from electrode, x, as well on the temperature. Eq. (6) is significantly different from the classic equilibrium of drift and diffusion when the external electric field is applied. In the case of thermoelectricity in nanoporous proton-conductive materials, the ionic flow due to the temperature gradient (right side of Eq. (6) compensates and overrides the sum of diffusion due to the concentration gradient and the electric-field-supported drift current, as shown in Fig. 3.

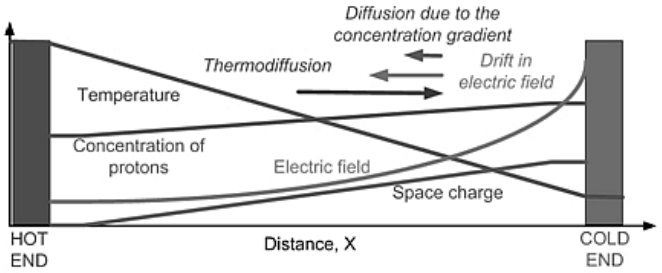

Fig. 3. Schematic of gradients and currents in the nanoporous protonic thermoelectric cell.

While the thermal gradient can be assumed to be constant (i.e., linear decrement of temperature with distance) and thus the dependence of proton concentration on the temperature due to the dissociation of water would be accounted for, the major challenge is the interconnection between the concentration of protons and the electrochemical potential, φ. While this relationship is defined by the exponential function $n = n_0 \exp(q\varphi/kT)$ for the open circuit, due to the compensation of drift and diffusion flows, the loaded regime requires the net current, so Eq. (3) cannot be applied. Therefore, Eq. (6) should be accompanied by at least one more equation to connect the concentration of protons with the temperature gradient and/or electrochemical potential. For this purpose, the space charge density, ρ, the Poisson equation should be defined as the difference between the concentrations of hydronium, H_3O+, and hydroxyl, OH^-, ions. When the local concentration of protons is increased due to thermodiffusion, this affects the local equilibrium in water dissociation, the mass balance constant of which depends on local temperatures.

The basic expression for the thermionic current density (6) can be rewritten in the phenomenological form by the using coefficients for thermodiffusion, mobility and self-diffusion of charge carriers as

$$j = q\gamma n\frac{dT}{dx} + qn\mu E + qD\frac{dn}{dx} \ , \qquad (7)$$

where γ is the coefficient of thermodiffusion (to be defined), μ is the mobility of protons, and the self-diffusion coefficient, D, may be expressed through the mobility according with Einstein–Smoluchowski relation for diffusion of charged particles $D = \mu_q kT/q$. Coefficients of thermodiffusion, mobility and self-diffusion may be defined as partial derivatives of current (see Eq. 7) for varied temperature and electric field correspondingly. The resulting expression are:

coefficient of thermodiffusion, $\gamma = f\exp(-\frac{W_b}{kT})\frac{\delta W_b}{kT^2}$, (8)

and mobility, $\gamma = f\exp(-\frac{W_b}{kT})\frac{\delta W_b}{kT^2}$. (9)

Therefore, $\gamma = \frac{\mu W_b}{q\delta T}$. (10)

The numerical analysis was performed by the digital modeling of Eq. 7 with accounting for equations from 8 to 10 at the uniform gradient of temperature. Results of this modeling are presented in Fig. 4 and 5.

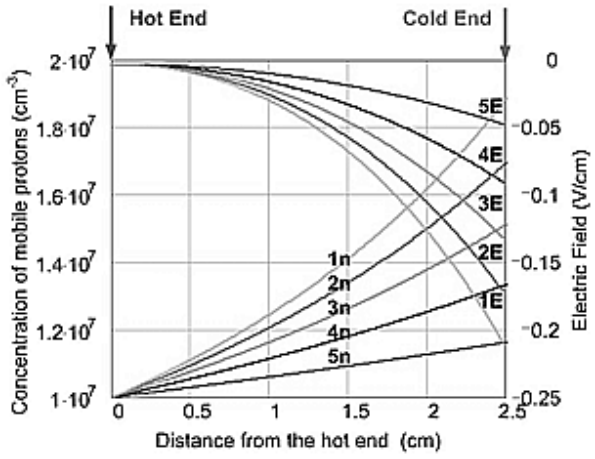

Fig. 4. Modeled profile of the concentration of mobile protons, n, and electric field , E, between electrodes of at varied gradient of temperature:1 – 6 K/cm; 2 – 12 K/cm; 3- 18 K/cm; 4 – 24 K/cm; and 5 – 30 K/cm.

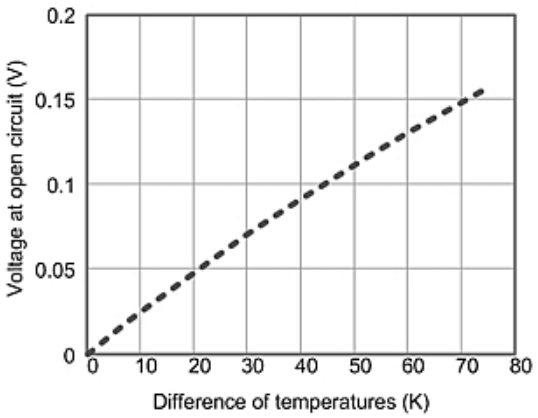

Fig. 5. Modeled thermoelectric voltage on electrodes at varied difference of temperatures.

Fig.4 and 5 show that while the electric potential profile is highly non-linear despite of the supposed uniform gradient of temperature, the resulting electromotive force (voltage on electrodes at the open circuit) follows the temperature difference almost linearly. Therefore, the Seebeck coefficient, $S = \Delta V/\Delta T$, is practically constant in the temperature range in interest, form 300K to 400K. The estimation for dimensionless figure of merit for the thermoelectric generator, $ZT = S2\sigma T/\kappa$, requires the ratio of electric and thermal conductivities, σ/κ which should be defined experimentally because it depends on material of electrodes and thermal design of the cell.

III. EXPERIMENTS

Initial tests were performed with a semi-dry cell with deionized (DI) water inside a thin layer of a polyvinyl alcohol (PVA) sponge. This cell is shown in Fig. 6. Electrodes were made from calendered (pressed through rollers) graphite. A temperature gradient was created using two aluminum thermal buses with (TE) modules, which cooled the sample at one end and heated it at the other end. To ensure that the electrodes were isolated from leakage of current from the thermoelectric modules, thin (75 μm) layers of Kapton (polyimide) were installed between the cell sandwich and these modules. All of the thermoelectric modules were electrically connected in series so they generated the same heat flux. Because of the internal heat loss in each TE cooler, the released heat exceeded the extracted heat. This extra heat was rejected to the ambient air by aluminum buses, which served as heat sinks. To increase the release of this heat, the aluminum buses were held in place by a laboratory vise that served as a heat drain. The temperature of the electrodes was controlled by K-type thermocouples.

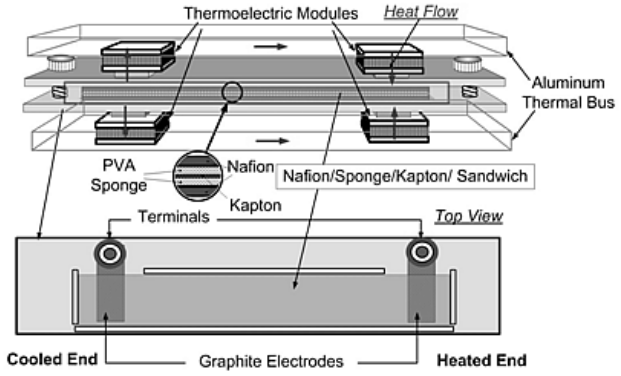

Fig. 6. Schematic of the initial prototype

The tested material was obtained from Ion Power, Inc., which is a distributor of DuPont Nafion®. Membrane type N 117 typically has a thickness of 183 μm, conductivity of ~0.1 S/cm (submersed in 25°C deionized water), and water uptake (ASTM D 570) of 38%. Being water soaked, the membrane expanded in all dimensions (thickness and length) by ~10% at 23°C (by ~15% at 100°C). Samples of material were cut into 25 mm × 75 mm strips. Because the electrodes used were 25 mm × 25 mm, the temperature gradient was created on a length of 25 mm. This temperature gradient was varied by the changing of the current through the thermoelectric modules, and the voltage on the electrodes was measured using a digital oscilloscope connected through a microampermeter. The generated open circuit thermoelectric voltage was measured using a DC regime in the oscilloscope (1 MOhm input impedance). In this regime, the current was less than 100 nA. Each measurement was taken with temperatures and voltages completely established. To exclude the effect of residual voltage from the accumulation of hydrogen near the bulk graphite electrode, each cycle of measurements, i.e., increasing and decreasing the temperature gradient, was done with a fresh Nafion® sample. Fig. 7 shows the averaged thermoelectric output characteristic obtained from five samples.

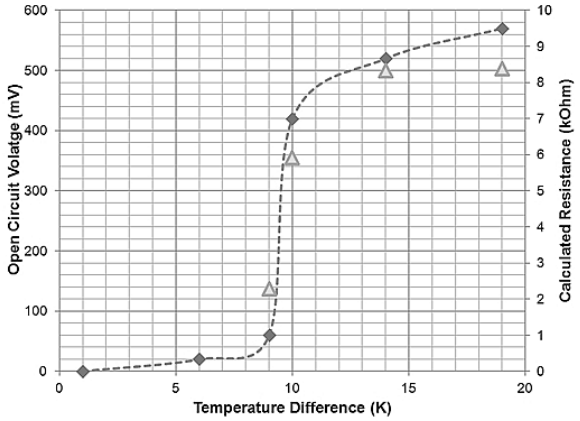

Fig. 7. Open circuit voltage on graphite electrodes with Nafion® film samples.

The "jump" in the output voltage at the temperature difference, ~10K, and a voltage level of ~60 mV, can't be attributed to an accumulation (charge or hydrogen) effect because the characteristic, shown in Fig. 7, is completely reversible. This "jump" was explained by the diode-like non-linearity of the contact resistance between the ion-conductive material and the graphite electrodes. At a low generated voltage, these contacts are practically closed (current is low) and the generated voltage is distributed between the internal resistance of the cell, these contacts, and the external load (oscilloscope input impedance). The generated electromotive force (e.m.f.) is equal to the sum of the voltages applied to the material in the cell, the contacts, and the external load, but has the opposite polarity. Because the oscilloscope shows only the voltage applied to the input impedance, the drop in electric potential on the contacts is subtracted from the generated e.m.f.. When the voltage on the contacts increases beyond the threshold level, the contact resistance sharply decreases and most of the e.m.f. is applied to the oscilloscope, which has a significantly higher input impedance than the impedance of the material in the cell. As Fig. 7 shows, the actual impedance of the cell (excluding the contact effects at low voltages) is ~8.5 kOhms. This value was checked with a polarimetric test of the cell, as shown in Fig. 8.

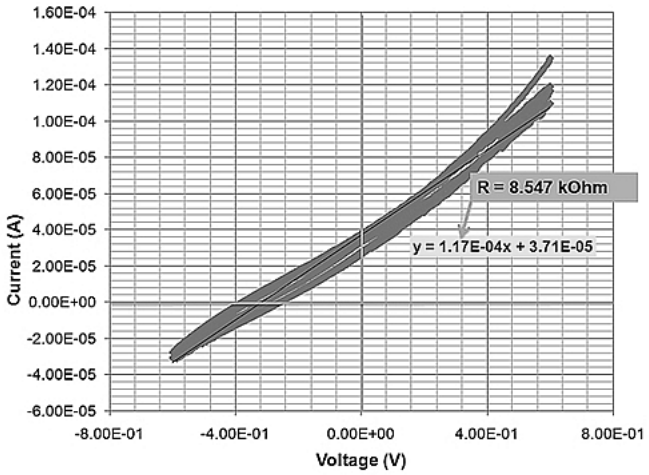

Fig. 8. Polarimetric test of the Nafion®-based cell shown in Fig. 6.

A polarimetric cycling test with a voltage amplitude of 65 mV showed the effective impedance of the cell as 8.547 kOhms, which correlates to the calculated resistance in Fig. 7. To evaluate the maximal power output from the experimental cell shown in Fig. 6, we loaded the cell by the 10 kOhm resistor, which closely matched the internal impedance. The results of this test are shown in Fig. 9, which shows that the thermoelectric voltage is saturated at ~64 mV in the temperature difference range of 10 K to at least 22 K. After that, the output voltage sharply increases – almost twofold. Despite the similarity of plots, this "jump" in voltage cannot be attributed to contact barriers because the density of current is significant (see the output power density in Fig. 7). Instead, we have explained it as attributable to the establishment of the flow of hydrogen from the anode to the cathode; this flow requires a significant concentration of hydrogen near the anode to penetrate the squeezed PVA sponge. The accumulation of hydrogen on the anode explains the "plateau" in the characteristics shown in Fig. 7: The cathode area is depleted by mobile protons and their generation by thermal water dissociation.

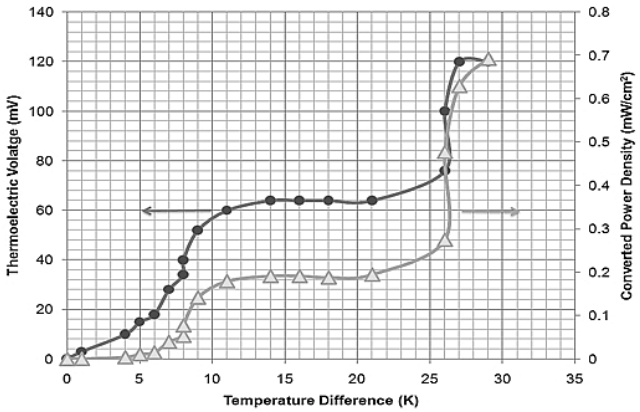

Fig. 7. Thermoelectric voltage and power density of Nafion® samples at an external load 10 kOhms.

To avoid these limitations, a new conceptual prototype of the ionic thermoelectric cell was designed and built (see Fig. 8).

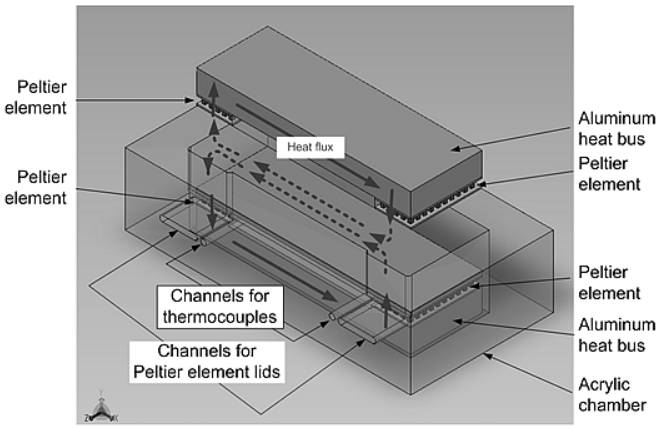

Fig. 8. Schematic of the improved ionic thermoelectric cell.

This new, improved cell was intended to be used with palladium hydride electrodes, which provide low contact resistance between the electrode and the electrolyte. Copper electrodes were fabricated using printed circuit board (PCB) technology, electroplated with an 80 nm layer of palladium and saturated with hydrogen by electrolysis in a weak acidity

(pH 6) buffer to create palladium hydride, PdHx. Some electrodes were machined to create additional longitudinal grooves for the circulation of hydrogen.

To support multiple tests (for attaining the established steady state), an automated setup was built using NI LabVIEW software installed on the laboratory computer. This setup allowed the voltage applied to the TE modules to be automatically ON and OFF over varying periods of time and facilitated the recording of the voltage and current output as well as the temperature at the hot and cold ends of the cell. Later, this setup was enhanced by the addition of a heat flux sensor (RdF 27160) to monitor the heat flux through the cell.

Fifteen samples of Nafion® were tested with Pd-coated electrodes (five without grooves and 10 with grooves). No notable effect of the grooves was detected. The averaged characteristics for these tests are shown in Fig. 9 and 10.

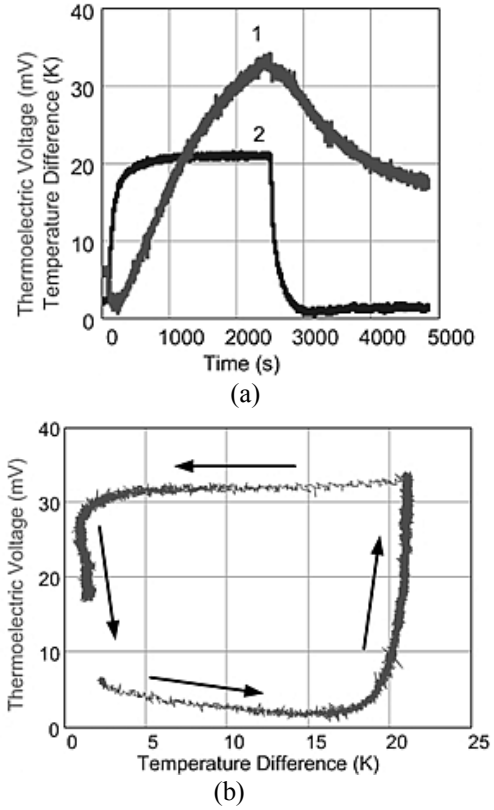

Fig. 9. Test results obtained with Nafion® media and Pd-coated electrodes: (a) shape of the established thermoelectric voltage (1) and temperature difference (2) pulses; (b) dependence of thermoelectric voltage on the temperature difference between electrodes.

As Fig. 9(a) shows, the measured Seebeck coefficient with PdHx-coated electrodes is limited to ~1.5, while graphite electrodes demonstrated the Seebeck coefficient in excess of 4 (see Fig. 7). Fig. 9(a) also shows that the voltage never saturates over the 40 min period. This can be explained by the slow buildup of hydrogen content in the anode coating, i.e., a significant amount of protons was excluded from the external circuit, lowering the thermoelectric output. This conclusion is supported by the phenomenon of slow charging of the tested cell, as shown in Fig. 10.

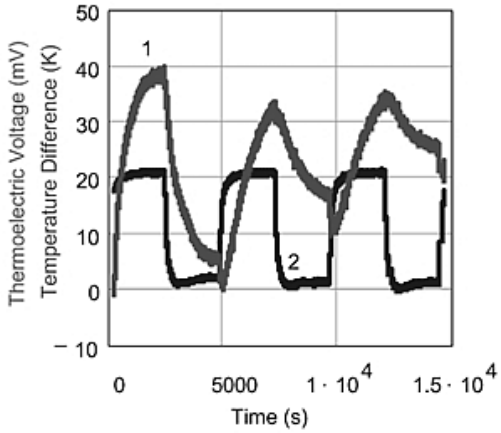

Fig. 10. Shape of the thermoelectric voltage (1) and the temperature difference (2) pulses during saturation of PdHx coating by protons.

Fig. 10 shows that while the initial Seebeck coefficient with PdHx electrodes reaches 2 mV/K, it gradually decreases with time, while the residual voltage (output at zero temperature difference) increases. Interestingly, the density of the accumulated charge is large enough, and the carriers of the charge are bound to deep traps, so that the residual voltage decreases by only 8-10% when electrodes were shortened overnight (8 hours) at room temperature (22□C). Heating the "charged" cell to 60°C improved the relaxation of this "charge" to ~40% per hour. While this "charging of the proton battery" may be an interesting phenomenon for practical applications (e.g., energy storage for solar powered converters), it creates a significant measurement challenge because the sample has a "memory of prehistory." For this reason, the following experiments were conducted using carbon fiber electrodes. Fig. 11 and 12 show the averaged characteristics of the cell using 12 samples of fresh Nafion® film and fresh carbon fiber electrodes.

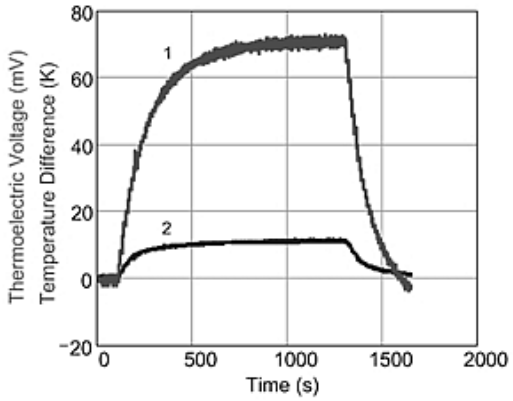

Fig. 11. The shape of the established thermoelectric voltage (1) and the temperature difference (2) pulses obtained with fresh Nafion® media and fresh carbon fiber electrodes.

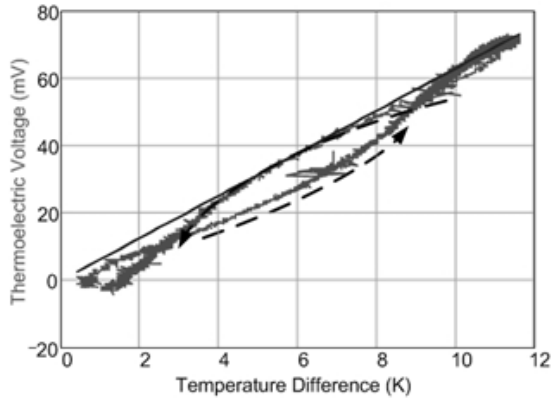

Fig. 12. Dependence of thermoelectric voltage on the temperature difference between the electrodes obtained with fresh Nafion® media and fresh carbon fiber electrodes.

As Fig. 12 demonstrates, the process using fresh electrodes and polymer samples is reversible, and the Seebeck coefficient over 6 mV/K is achievable. Nevertheless, if the Nafion® samples go through multiple temperature cycling, the thermoelectric output decreases to 4 mV/K, as shown in Fig. 13.

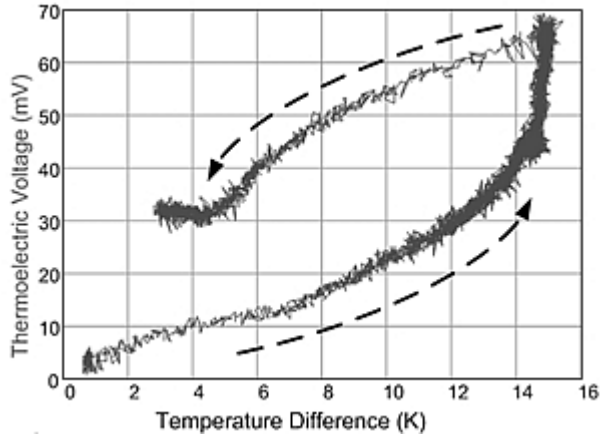

Fig. 13. Dependence of thermoelectric voltage on the temperature difference between the electrodes obtained with fresh Nafion® media and 'aged' carbon fiber electrodes

Fig. 13 shows notable residual voltage (about half of the maximal voltage). We concluded that this "aging" of the cell is related to the limited diffusion of hydrogen along the electrode. Because the reduction of protons starts at the front edge of the electrode, the concentration of hydrogen there is maximal, which blocks the diffusion of hydrogen released in the middle of the electrode.

To improve the diffusion of hydrogen an decrease the resistance of cell, we have fabricated the thermoelectric cell from Nafion® N117 film with carbon fiber electrodes and a PVA wet sponge spacer. These components comprised the prototype insert, which was made by rolling the strip, as shown in Fig. 14. The carbon electrodes in the rolled insert were wrapped in copper bands, both to hold the roll and to provide the capability to solder on wire terminals. The insert was then placed in the polyethylene tube, with wires inserted through the holes in the tube. Alumina plates were mounted on the ends, which served as thermal terminals and seals for the device that is shown in Fig. 15.

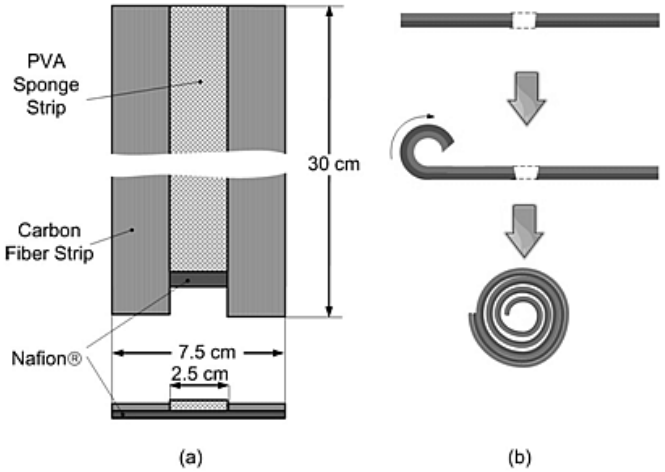

Fig. 14. Fabrication of the rolled insert for the thermoelectric cell: (a) assembling of composite strip; (b) rolling of insert.

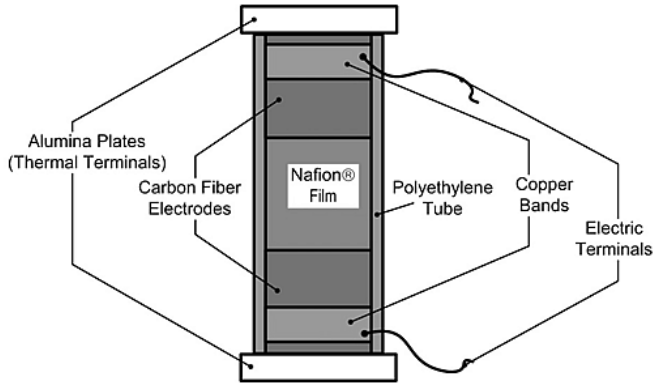

Fig. 15. Structure of the improved thermoelectric cell.

Improved cells in open circuit regime demonstrated the Seebeck coefficient ~ 4.5 as shown in Fig. 16.

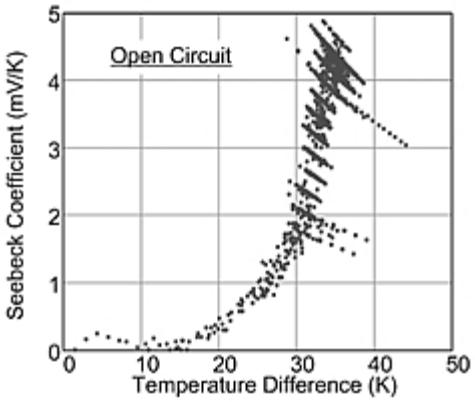

Fig. 16. Seebeck coefficient vs the temperature difference along the cell with the open circuit.

The thermoelectric output voltage with a matching load for the cycled temperature difference is presented in Fig. 17.

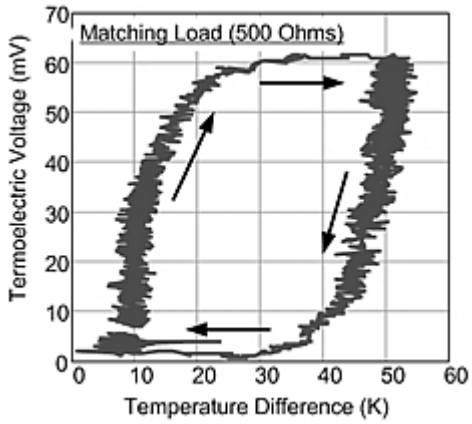

Fig. 17. Thermoelectric output voltage from the cell with a matching load at the cycled temperature difference.

While the maximal voltage on the matching load is significantly lower that with open circuit, effects of the saturation of voltage and residual voltage are clearly notable in Fig. 17. Fig. 18 shows how the heat flux through the cell varies with the thermoelectric voltage.

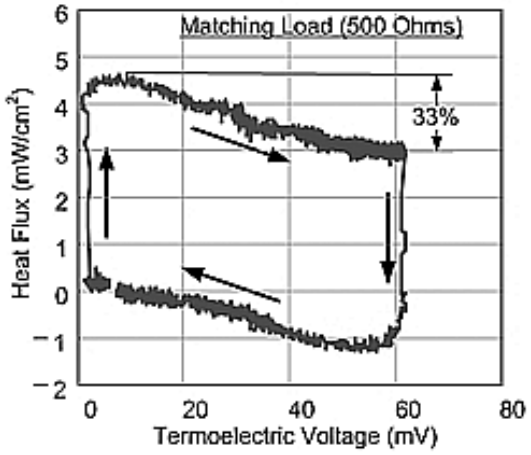

Fig. 18. Heat flux through the cell during the cyclic variation of temperature difference.

Fig. 18 shows a notable drop in the heat flux that correlates to the generated thermoelectric power. Initial drop of the heat flux is related to the thermoelectric power conversion. Because simultaneously the residual space charge is built, it creates the opposite heat flow (note the change of sign for the heat flux) until the space charge decays.

IV. Conclusions

We developed a basic model of the ionic thermoelectric device, built and evaluated the first thermoelectric cells, and thoroughly tested the prototype in varied temperature ranges and thermal loads. Other findings of this work include a significant thermogalvanic effect using carbon fiber electrodes, an accumulation of power with palladium hydride electrodes, and the effects of the contact electrochemical potential both on the generated thermoelectric voltage and the output impedance of the device.

References

[1] "Thermally-Activated Technologies: Technology Roadmap," U.S. DOE Office of Energy Efficiency and Renewable Energy, 2003.

[2] G. Foley, R. DeVault, R. Sweetser, "The Future of Absorbtion Technology in America," ABST-2000 Conference, Washington, DC, June 6-8 2000, Oak Ridge National Laboratory, 2000.

[3] "Market Potential for Advanced Thermally Activated BCHP in Five National Account Sectors," Energy and Environmental Analysis, Inc., Arlington, VA, 2003.

[4] D.A. Relay, "Heat Recovery Systems," E&F.N.Span, London, 1979.

[5] M.S. Dresselhaus, Y.M. Lin, S.B. Cronin, M.R. Black, O. Rabin, and G. Dresselhaus, "Investigation of Low-dimensional Thermoelectric," Nonlithographic and Lithographic Methods for Nanofabrication: Symposium Proceedings, Steven Smith ed., Technomic Publishing Co., Inc., Lancaster, PA, 2001.

[6] S.B. Cronin, Y.-M. Lin, O. Rabin, M.R. Black, and M.S. Dresselhaus, "Thermoelectric Transport Properties of Bismuth Nanowires," The 21st International Conference on Thermoelectrics: ICT Symposium Proceedings, Long Beach, CA, T. Caillat and J. Snyder eds., IEEE, Piscataway, NJ, pp. 243-248, 2002.

[7] B.R. Brown, M.E. Hughes, and C. Russo, "Thermoelectricity in Natural and Synthetic Hydrogels," Phys. Rev. E, 70, 031917, 2004.

[8] M. Reznikov and A. Kolessov, "Space Charge Effects in the Electrolytes," Proc. of Electrostatics Joint Conference, ESA/IEA/IEJ/IAS/SFE, Boston, June 2009.

[9] M. Reznikov, "Thermoelectric Power by the Diffusion of Protons in a Nanoporous Structure," Mater. Res. Soc. Symp. Proc., vol. 1325 © 2011 Materials Research Society, DOI: 10.1557/opl.2011.1116.

[10] J. Janek and C. Korte, "Thermal Diffusion in Mixed Conductors," Proc. Electrochem. Soc., vol. 97, no. 24, pp. 304-328, 1998.

[11] P. Choi, N. H. Jalani, and R. Datta, "Thermodynamics and Proton Transport in Nafion II. Proton Diffusion Mechanisms and Conductivity," Journal of the Electrochemical Society, vol. 152 (3), E123-E130, 2005.

[12] J.N. Agar, "Thermogalvanic Cells," Advanced in Electrochemistry and Electrochemical Engineering, P. Delahay and C. W. Tobias, eds., vol. 3, p. 31, Interscience, New York, 1963.

[13] A.V. Sokirko, "Theoretical Study of Thermogalvanic Cells in Steady State," Electrochimica Acta, vol. 39, no. 4, pp. 597-609, 1994.

[14] J.W. Tester, U. Holeschovsky, K.C. Link, and J. Corbett, "Evaluation of Thermogalvanic Cells for the Conversion of Heat to Electricity," MIT-EL 92-007, 1992.